Mutual Interaction between Superconductors and Ferromagnetic Skyrmionic Structures in Confined Geometries

Leonardo González-Gómez, Josep Castell-Queralt, Nuria Del-Valle, and Carles Navau*
Departament de Física, Universitat Autònoma de Barcelona, 08193 Bellaterra, Barcelona, Catalonia, Spain

(Received 16 August 2021; revised 18 January 2022; accepted 11 March 2022; published 29 March 2022)

The mutual interaction between a chiral ferromagnetic disk with confined skyrmionic structures and a superconducting disk is studied. The interaction is accounted for by solving simultaneously the Brown and London equations. We find that for a superconductor under an applied uniform field, the stray field of the shielding currents can trigger switching between different skyrmionic states in the ferromagnet that is not possible without the superconductor. We discuss the effect of the different parameters on the results and some possible applications such as multivalued logic, storage, and skyrmionic metamaterials.

DOI: 10.1103/PhysRevApplied.17.034069

I. INTRODUCTION

Interaction between ferromagnets (FMs) and superconductors (SCs) has received much attention both from a theoretical and an applied point of view over the past decades [1–5].

At the nanometric scale, the magnetization distribution of the FM tends to be homogeneous due to the increasing relative importance of the exchange interaction with respect to the demagnetizing field. In spite of this, in ferromagnetic films in contact with heavy metals with strong spin-orbit coupling, the interfacial Dzyaloshinskii-Moriya (IDM) interaction can lead to the stabilization of skyrmions, which are twisting magnetization textures with sizes on the order of few tens of nanometers [6–9]. Moreover, when confined in a nanometric dot, the boundaries offer extra stabilization to such structures and other skyrmioniclike textures may be stable. The morphology of the structures depends not only on the material interactions and the applied field but also on the confining geometry [10–16].

As for the superconducting layers, it is well known that they react to changes in the environmental magnetic field in a diamagnetic way. As a consequence, the response of the SC depends on the environmental field present when the sample is cooled below its transition temperature. In this sense, it is common to separate the field-cooled from the zero-field-cooled case, depending on whether or not there is an external field when the sample transits to the superconducting state. In addition, in type-II superconductors, circulating currents, called superconducting vortices, can appear that allow the presence of a magnetic induction field in the interior of the superconductor with a quantized value of the magnetic flux [17,18].

Several works have been devoted to the study of the FM/SC interaction with topological defects, among which are the Abrikosov (bulk samples) and Pearl (thin samples) vortices in type-II SCs or magnetic domain walls and skyrmions in FMs. These FM/SC heterostructures have been envisaged for different applications, such as the manipulation of superconducting properties (vortex dynamics, critical currents, etc.), the study of spin-injection phenomena, Josephson devices, achieving topological superconductivity for topological quantum computing, the imprinting of ferromagnetic states or vortices in the SC, and spintronics [2,19–28], among many others. In particular, it has been found that Pearl and Abrikosov vortices can be spontaneously nucleated due to a topological defect in the FM (domain walls or skyrmions) [25–27,29–34].

Beyond interaction via the proximity effect (where the superconducting wave functions extends to the FM and the Cooper pairs diffuse into it [35]), the interaction via the stray field between a ferromagnetic skyrmionic structure and a close superconducting element has received attention recently [27,32,33,36–39]. In all these works, one of the elements is considered fixed (the SC currents or the FM magnetization), while the other is relaxed (the FM magnetization or the SC currents are found) under the effect of the stray field of the fixed element. This approach is viable when a one-way coupling is justifiable. Furthermore, we found no systematic works considering finite geometries of both the FM and the SC.

Here, we consider the *mutual* interaction between *confined* skyrmioniclike structures and superconducting currents, in a FM/SC bilayer system and find that these systems can exhibit a rich phenomenology of different

*carles.navau@uab.cat

magnetization states in the FM, triggered by the shielding currents induced in the SC.

The presented results show the possibility of achieving several well-defined (large range of applied fields), stable, and accessible magnetization states that could be used for multivalued logic devices or for increasing the magnetic information storage capacity. In addition, the studied system can be used as basic elements for larger systems, the effective properties of which could be geometrically tuned [40,41], even in a nonlinear and anisotropic way.

The paper is structured as follows. In Sec. II, we introduce the model used for the calculations, with special focus on the approximation done and the equations used. In Sec. III, we present the obtained results for the magnetization for different applied fields and how the system evolves when one state becomes unstable. In Sec. IV, we discuss the magnetization loops and the current distribution as well as the dependence on the parameters. Finally, we present our conclusions in Sec. V.

II. MODEL

A. Physical description

Consider a superconducting planar thin disk of radius R_s and thickness $t_s \ll R_s$, centered at the origin of the coordinates and on the $z = 0$ plane. Coaxial and parallel to it, a ferromagnetic thin disk, of radius R_f and thickness $t_f \ll R_f$ is located, with its center at $d\hat{\mathbf{z}}$ (see Fig. 1). Consider that this FM is coupled with heavy-metal samples that provide IDM interaction that allows us to stabilize Néel skyrmions, as well as 2π state (target skyrmion) or other skyrmionic structures [10].

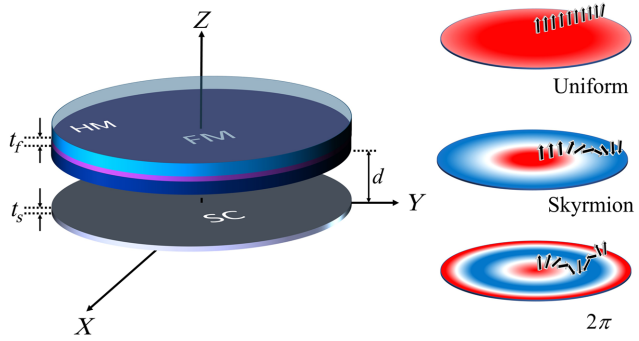

FIG. 1. Left: a sketch of the studied system: a superconducting disk (gray) coaxial to a ferromagnetic disk (purple) with IDM interaction due to two different attached heavy-metal layers (blue). The ferromagnetic and superconducting disks are separated by a distance d. Both disks are considered ultrathin. Right: a sketch of the skyrmionic structures in the ferromagnetic layer found and studied in this work. The colors represent the z component of the magnetization and the arrows the local magnetization along the radius.

We model the SC within the London approximation, which is characterized by a London penetration depth λ [17,18]. We consider that the currents flow in the superconductor homogeneously across the thickness, so that we define an axisymmetric sheet-current density $\mathbf{K}(\rho) = \int_{-t_s/2}^{t_s/2} \mathbf{J}(\rho, z)\, dz$. $\mathbf{J}(\rho, z)$ is the current density inside the superconductor and ρ is the radial coordinate. Because of the symmetry, the sheet-current density has only an angular component $\mathbf{K}(\rho) = K_\phi(\rho)\hat{\boldsymbol{\phi}}$. The sheet-current distribution is determined by the potential vectors due to the current in the SC ($\mathbf{A}_k$), the magnetization of the FM ($\mathbf{A}_m$), and the applied field ($\mathbf{A}_a$). We define the screening length $\Lambda = 2\lambda^2/t_s$ [42,43].

The micromagnetic model is used in the FM, where the magnetization is considered to be uniform in magnitude all over the sample and not varying across its thickness. Thus, the magnetization is considered to be $\mathbf{M}(\rho) = M_s\mathbf{m}(\rho)$, where M_s is the saturation magnetization and $\mathbf{m} = (\sin\theta\cos\varphi, \sin\theta\sin\varphi, \cos\theta)$ is a dimensionless unit vector determining the magnetization direction. θ and φ are the polar and azimuthal angles describing the direction of the magnetic moment. We consider that the internal magnetic structure of the FM is determined by the local exchange field ($\mathbf{H}_{\text{ex}}$), the IDM field ($\mathbf{H}_{\text{DM}}$), the uniaxial out-of-plane anisotropy field ($\mathbf{H}_{\text{an}}$), the stray field coming from the currents in the SC ($\mathbf{H}_k$), and a uniform applied field ($\mathbf{H}_a$). The demagnetizing field is considered to be renormalized in the uniaxial anisotropy [44–46]. To ensure the validity of this approximation for our finite samples, the demagnetizing field of the structures is computed. It is found that its z component is approximately proportional to m_z, justifying the renormalization. To focus the treatment, we consider Néel skyrmionic structures with the magnetization core pointing to $+\hat{\mathbf{z}}$ and a perpendicular applied field $\mathbf{H}_a = H_a\hat{\mathbf{z}}$.

B. Formulation

Our model allows us to find the equilibrium magnetization distribution in the FM and the current distribution in the SC, *simultaneously*. They are determined by using the London equation inside the SC [17] and the static Brown equation in the FM [47]. That is,

$$\begin{cases} \mathbf{K} = -\dfrac{2}{\mu_0\Lambda}\mathbf{A}, & \text{for } z = 0 \text{ and } \rho < R_s, \\ \mathbf{M}\times\mathbf{H}_{\text{eff}} = 0, & \text{for } z = d \text{ and } \rho < R_f, \end{cases} \tag{1}$$

where $\mathbf{A}$ is the total magnetic vector potential in the SC and $\mathbf{H}_{\text{eff}}$ the total effective field in the FM:

$$\mathbf{A} = \mathbf{A}_k + \mathbf{A}_m + \mathbf{A}_a, \tag{2}$$

$$\mathbf{H}_{\text{eff}} = \mathbf{H}_{\text{ex}} + \mathbf{H}_{\text{DM}} + \mathbf{H}_{\text{an}} + \mathbf{H}_k + \mathbf{H}_a. \tag{3}$$

The vector potential created by the currents in the superconductor at any point is evaluated from

$$\mathbf{A}_k(\rho,z) = \hat{\boldsymbol{\phi}}\frac{\mu_0}{4\pi}\int_0^{R_s} K_\phi(\rho')Q(\rho,\rho',z)\rho' d\rho', \quad (4)$$

where

$$Q(\rho,\rho',z) = \int_0^{2\pi} \frac{\cos\phi'}{\sqrt{\rho^2+z^2+\rho'^2-2\rho\rho'\cos\phi'}}\, d\phi'. \quad (5)$$

Actually, this integral can be done analytically in terms of elliptic functions, although for most purposes it is convenient to evaluate it numerically. The magnetic field created by these currents at the FM (outside the SC) is

$$\mathbf{H}_k(\rho,d) = \frac{1}{\mu_0}\left(\nabla\times\mathbf{A}_k\right)|_{(\rho,d)}. \quad (6)$$

The vector potential due to the magnetization distribution in the FM can be evaluated, at the SC, as

$$\begin{aligned}\mathbf{A}_m(\rho,0) = \frac{\mu_0}{4\pi}t_f\Bigg[&R_f M_z(R_f)Q(\rho,R_f,-d)\\ &+\int_0^{R_f} M_\rho(\rho')\left.\frac{\partial Q(\rho,\rho',z)}{\partial z}\right|_{z=-d}\rho'\,d\rho'\\ &-\int_0^{R_f}\frac{\partial M_z(\rho')}{\partial\rho'}Q(\rho,\rho',-d)\,\rho'\,d\rho'\Bigg]\hat{\boldsymbol{\phi}}. \quad (7)\end{aligned}$$

The applied vector potential is

$$\mathbf{A}_a = (1/2)\mu_0\mathbf{H}_a\times\mathbf{r} = (1/2)\mu_0\rho H_a\hat{\boldsymbol{\phi}}. \quad (8)$$

The rest of the fields that are involved are as follows:

$$\mathbf{H}_{\rm ex} = \frac{2A_{\rm ex}}{\mu_0 M_s^2}\nabla^2\mathbf{M}, \quad (9)$$

$$\mathbf{H}_{\rm DM} = \frac{2D_{\rm DM}}{\mu_0 M_s^2}\left[(\nabla\cdot\mathbf{M})\hat{\mathbf{z}} - \nabla M_z\right], \quad (10)$$

$$\mathbf{H}_{\rm an} = \frac{2K_{\rm an}}{\mu_0 M_s^2}M_z\hat{\mathbf{z}}, \quad (11)$$

where $A_{\rm ex}$, $D_{\rm DM}$, and $K_{\rm an}$ are the exchange, IDM, and uniaxial anisotropy constants, respectively. The boundary condition of the FM is $d\theta/d\rho|_{\rho=R_f} = D_{\rm DM}/2A_{\rm ex}$ [10].

The interaction between the SC and the FM is evidenced in the $\mathbf{A}_m$ and $\mathbf{H}_k$ terms. As we focus on the change in the magnetization states in the FM, after solving the system of Eq. (1), we evaluate the magnitude

$$\begin{aligned}E_m = t_f\int_0^{R_f}\Bigg(&\frac{A_{\rm ex}}{M_s^2}(\nabla\mathbf{M})^2 - \frac{K_{\rm an}}{M_s^2}M_z^2\\ &+\frac{D_{\rm DM}}{M_s^2}[\mathbf{M}\cdot(\nabla M_z) - M_z(\nabla\cdot\mathbf{M})]\\ &-\mathbf{M}\cdot\mathbf{H}_a - \frac{1}{2}\mathbf{M}\cdot\mathbf{H}_k\Bigg)2\pi\,\rho\,d\rho, \quad (12)\end{aligned}$$

which accounts for the magnetic energy due to the magnetization in the FM.

Note that the presence of the SC not only affects the last term in Eq. (12) but also contributes to changing the other terms by modifying the magnetization distribution (with respect to the case without the SC).

III. NUMERICAL RESULTS

A. Magnetization states for different applied fields

The system of Eq. (1) is solved numerically. It is important to remark that when discretizing the system, the kernel function Q becomes a matrix the diagonal elements of which strictly diverge when $z = 0$ (i.e., when evaluating the vector potential created by the SC on the superconducting points). To avoid this discretization problem, we follow Ref. [48], where these diagonal terms are evaluated. After discretization, the London equation becomes a system of linear equations that are solved using the Gauss-Seidel scheme. For the Brown equation, a relaxation method based on the Landau-Lifshitz-Gilbert equation with a high numerical damping constant is used [47] in order to speed up convergence to the solution while avoiding numerical instabilities. Both equations are iteratively solved until convergence [49]. We use the parameters found for Ta/Pt/Co/Ta/MgO/Pt multilayers [50]: $A_{\rm ex} = 15$ pJ/m, $D_{\rm DM} = 2.8$ mJ/m^2, $K_{\rm an} = 70$ KJ/m^3, and $M_s = 0.65$ MA/m. For the superconductor, we use the penetration depth $\lambda = 16$ nm of aluminum [51].

In general, there is a rich phenomenology that one can obtain depending on the distance d and also on the ratio R_f/R_s. We focus here on an interesting result that appears when the SC radius is larger than the FM one and they are quite close to each other. In particular, for the presented results, we set $t_f = 1$ nm, $R_f = 70$ nm, $R_s = 3R_f = 210$ nm, $d = 20$ nm, and $\Lambda = 24$ nm (we discuss the effect of these parameters below).

The possible stable states found for the studied system are shown in Fig. 2, for different applied fields. The states are represented by the averaged z component of the magnetization [Figs. 2(a) and 2(c)]. For a given field, one, two, or three states may be stable. The red, blue, and green lines correspond to the (quasi)uniform, the 2π, and the skyrmion state, respectively. It is seen that for large positive applied fields, the only stable structure is the (quasi)uniform state,

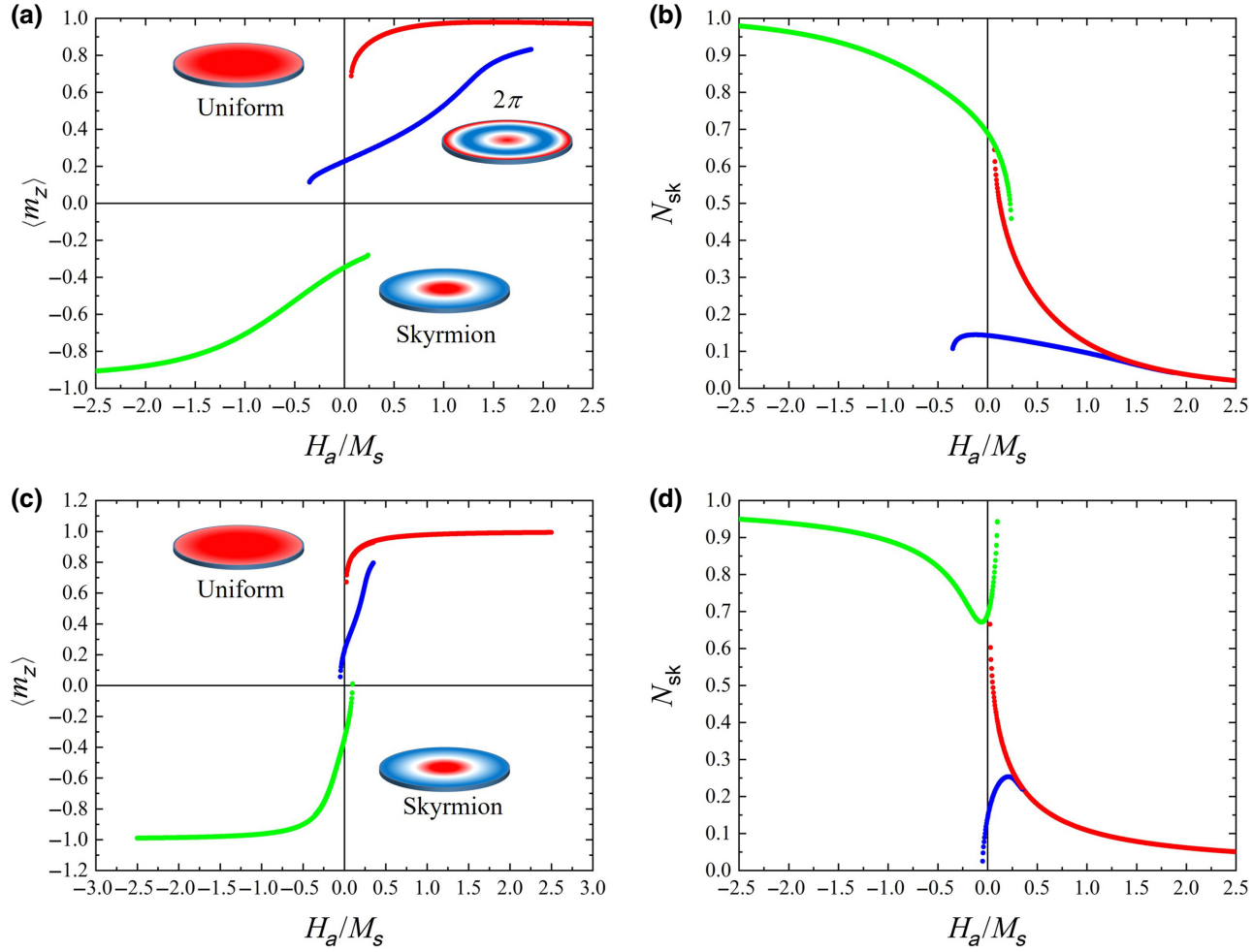

FIG. 2. The averaged z component of the normalized magnetization [(a),(c)] and of the skyrmionic number [(b),(d)], of all the stable magnetic states, for different applied fields in the presence [(a),(b)] and absence [(c),(d)] of the SC. The stable states found are the (quasi)uniform (red), skyrmion (green), and 2π (blue) states. A sketch of the magnetization distribution is shown in the magnetization panels.

while for large negative fields the only stable structure is the skyrmion (note that we assume that the center of the FM points in the positive z direction). There is a range of fields at which several structures are possible. What is interesting is that if the FM is at one state and the applied field changes quasistatically, this state will continue to be stable up to a critical value of the field. At that point, the system has to evolve to one of the other possible states for that field. One of the important differences due to the presence of the SC is that the range of fields where the 2π state could be stable has been greatly increased. But even more importantly, we see in the next subsection which transitions are allowed and to what state the system will evolve, and we see that the 2π state is accessible only in the presence of the SC.

To further characterize these different magnetic states, we also show the skyrmionic number [$N_{\mathrm{sk}} = 1/4\pi \int \mathbf{m} \cdot (\partial\mathbf{m}/\partial x \times \partial\mathbf{m}/\partial y)\, dxdy$], evaluated at different applied fields and for the cases with and without a SC [Figs. 2(b) and 2(d), respectively]. The skyrmionic number gives information on the topology of the structure. It represents the number of times spins wind around a unit sphere [52,53]. In ideal cases (infinite samples) the skyrmionic number is an integer, but in confined geometries this is no longer the case. In our example, the skyrmionic number of a (quasi)uniform state varies from zero (at large applied fields) to about 0.7 (at the fields at which this state is no longer stable). The 2π state, when stable, has a value that ranges from about 0.15 to zero. Note that the skyrmionic number as a function of the applied field behaves differently for the case with [Fig. 2(b)] and without a SC [Fig. 2(d)], specially for the skyrmion state.

B. GNEB analysis of the transitions between states

It must be noted that our procedure is unable to obtain the magnetization during the transitions from one state

to the other, since the calculations are based on the quasistatic finding of stable states. However, close to the transition, we can estimate the energy barriers by finding the minimum-energy path (MEP) between two stable magnetic structures. To follow an MEP in our system means to rotate spins in a way as to minimize the energy with respect to all degrees of freedom perpendicular to the reaction path. In order to estimate the different MEPs, we use the geodesic nudged elastic band (GNEB) algorithm [54] and compare the two possible transitions mediated by the magnetization boundaries. The GNEB algorithm is a quasistatic method by which we set an initial transition path (a discrete set of spin configurations interpolating between two stable states) that is iteratively optimized by zeroing the transverse component of the gradient force at each point along the path. This ensures the convergence to a first-order saddle point in the phase space, giving the MEP of the transition. Note that a displacement along the reaction path is a discrete analog of a reparametrization of the continuous path itself, so only transverse displacements of the path should be included [55].

In Fig. 3(a), we show the MEP found using the GNEB algorithm near the destabilizing field from the (quasi)uniform state to the 2π and the skyrmion states. It is found that when the field is approaching the destabilizing field ($H_a \simeq 0.07M_s$), the minimum corresponding to the (quasi)uniform state is becoming shallower up to disappearance. At that moment, it is clear from Fig. 3(a) that the most probable state is the skyrmion state. Actually, in that case the transition to the 2π state is found to go through an intermediate skyrmion state. Thus, when the (quasi)uniform state becomes unstable, the system will evolve to the skyrmion state. Once we are in the skyrmion state and we increase the field, this state can also be destabilized. For this case, in Fig. 3(b) we show the GNEB results for the MEP for the transitions to the (quasi)uniform and to the 2π states. In this case, again, when approaching the destabilizing field ($H_a \simeq 0.24M_s$), the minimum corresponding to the skyrmion state tends to disappear and when this happens it is clear that the most probable transition is to the 2π state. In this case, the energy barrier for this transition is smaller than the energy barrier for the skyrmion-to-uniform one, as is explicitly plotted in Fig. 3(c).

The same study is done for the case when there is no SC present in the system. In Fig. 4(a), the energy along

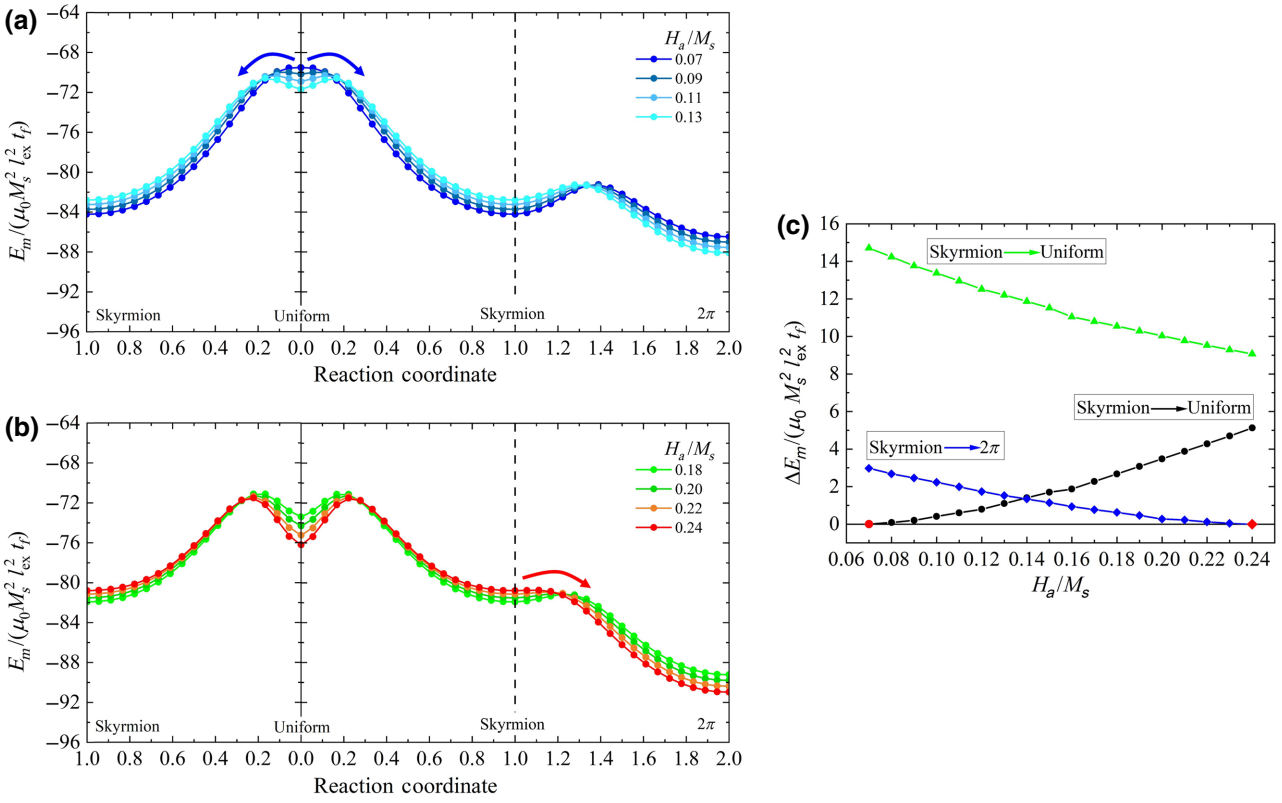

FIG. 3. The MEP calculated using the GNEB, showing the energy for the transitions occurring near the destabilization field of (a) (quasi)uniform and (b) skyrmion states, in the presence of a SC. The dots indicate the images computed along the converged path. The red arrows indicate the most probable transition found. (c) The energy barrier as a function of the applied field, for different transitions. The destabilizing fields at which the studied structures become unstable are highlighted in red. $l_{ex} = \sqrt{(2A_{ex})/(\mu_0 M_s^2)}$ is the exchange length.

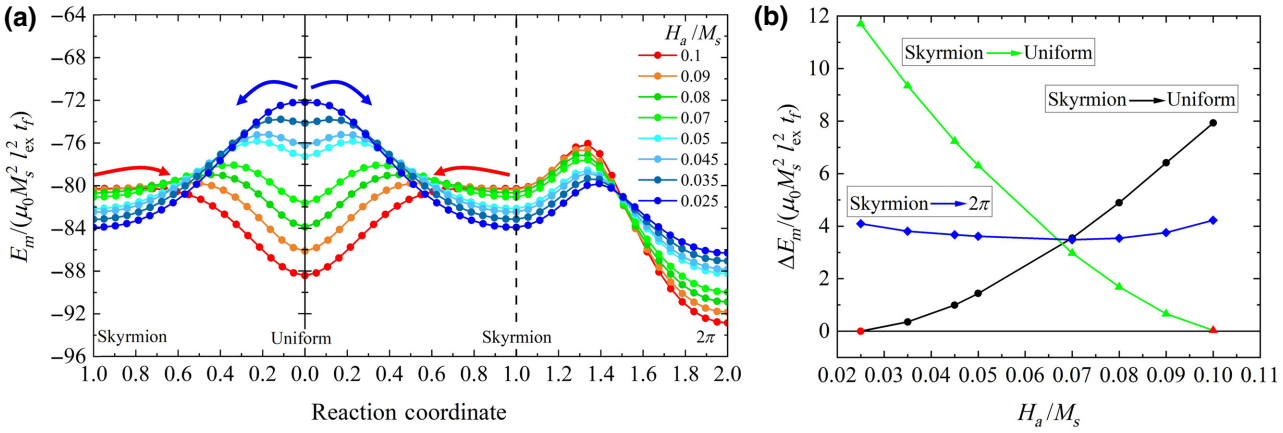

FIG. 4. (a) The MEP calculated using the GNEB, showing the energy for the transitions when there is no SC present, occurring at applied fields where the three states are stable ($0.025 < H_a/M_s < 0.1$). The dots indicate the images computed along the converged path. The blue and red arrows indicate the most probable transition found for that applied field. (b) The energy barrier as a function of the applied field, for different transitions. The destabilizing fields at which the studied structures become unstable are highlighted in red. $l_{ex} = \sqrt{(2A_{ex})/(\mu_0 M_s^2)}$ is the exchange length.

the reaction coordinate of the MEP is shown in the range of applied fields at which the three structures are found to be stable. We find that even though the 2π state might be stable, the transition to that state is less probable than its alternative near the skyrmion annihilation field. In this case, the energy barrier to transition to the 2π state is always bigger than the energy barrier of another transition, as is explicitly plotted in Fig. 4(b). Note that our model does not take temperature into account. The transition to the 2π state might be thermally activated in some cases but it will always be less probable than in the case where a SC is present [Figs. 3(a) and 4(a)]. Hence, the addition of a SC element significantly changes the energy landscape and possible transitions of the FM: an additional transition to the 2π state appears.

There are several considerations at this point. First, due to the symmetry of our system, since there cannot be a transition through the angular component of the magnetization, to transition from the (quasi)uniform to the 2π state, the magnetization must occur through an intermediate skyrmion state. Second, the energy barriers found using our implementation of the GNEB algorithm are evaluated within the micromagnetic approach. Hence, the effective field used to optimize the MEP is in the continuum approximation. As such, it does not take Bloch-point formation into account. However, in previous works [56,57] it has been found that, for finite samples (i.e., racetracks), the transition takes place through the boundaries of the FM and is not mediated by the formation or annihilation of a Bloch point. This justifies the fact that our calculations give an estimate of the stability and provides information on the most probable transition. Third, to strengthen this argument, we show in the Supplemental Material [58] some videos of the changes in the magnetization distribution following hysteresis loops (see Sec. IV A), where it becomes clear that the destabilization of the states is triggered mainly by a magnetization change at the borders of the FM, which further supports the GNEB findings.

IV. DISCUSSION

A. On the magnetization loops of the FM/SC hybrid system

The applied field is initially set at a very large value so that the ferromagnet is saturated in the uniform state, even with the presence of the zero-field-cooled SC. Two different quasistatic hysteresis loops are studied: an outer loop in the range $H_a = \pm 2.5 M_s$ and an inner loop in the range $H_a = \pm 0.75 M_s$. Both loops are presented in Fig. 5.

For the inner loop [Fig. 5(a)], we start from the saturated (quasi)uniform state and reduce the applied field. At slightly positive fields ($H_a \simeq 0.07 M_s$), the state is destabilized and transitions to the skyrmion state through the disk boundaries, as is found with the GNEB algorithm. Once in the skyrmion state, we reduce the applied field up to $H_a = -0.75 M_s$ and then increase the field to $H_a \simeq 0.24 M_s$, where the skyrmion state transitions to the 2π state. In this state, we increase the field up to $H_a = 0.75 M_s$, where the 2π state is still stable, and then reduce it to negative fields ($H_a \simeq -0.35 M_s$), where the system transitions to the skyrmion state, as it is the only stable state. In contrast, for the outer loop [Fig. 5(b)], the behavior of the system is similar to that for the inner loop but as the applied field is further increased ($H_a \simeq 1.88 M_s$), in the 2π state, the FM sample saturates to the (quasi)uniform state. Therefore, depending on the range of the hysteresis loops, two

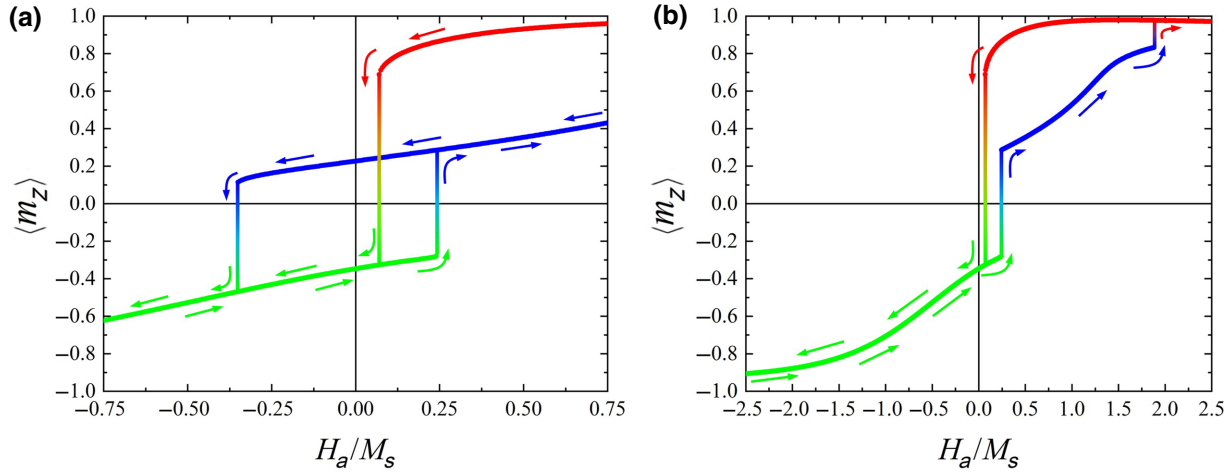

FIG. 5. The averaged z component of the normalized magnetization during the hysteresis loop. (a) The inner hysteresis loop with a field in the range $\pm 0.75 M_s$. (b) The outer hysteresis loop with a field in the range $\pm 2.5 M_s$. The vertical lines are sketched in gradient colors to indicate transitions between magnetization states: red for uniform, green for skyrmion, and blue for 2π.

different magnetization loops are found. Both loops are shown in the Supplemental Material [58].

We observe important facts when the SC is present: (i) the different magnetization states are stable for a large range of applied fields (although the local magnetization distribution changes slightly); (ii) the magnetic states are clearly distinguished by their average magnetization; and (iii) the presence of the SC drastically modifies the magnetization loop of the FM, as well as the skyrmionic number loop, allowing the FM to transit to an otherwise unreachable 2π state.

This last point is specially relevant: from the uniform state the system evolves to the skyrmion state and from the skyrmion state to the 2π state, but from the 2π state we can either go to the (quasi)uniform state or, if the field swept is reversed again before the destabilization at large fields, to the skyrmion state again.

We see that the transition to the 2π state (which would not happen without a SC) is triggered by the magnetization change at the border of the FM. The physical reason is that when the SC is present and close to the FM, the shielding due to the SC results in a significantly increased vertical field close to the edge of the FM and an additional radial field. This produces a large bending of the magnetization close to the borders that, eventually, results in the change to another magnetization state, favoring the 2π state. Both the presence of the SC and the confinement play a crucial role in the appearance of these states.

B. On the current distribution

During the whole magnetization loop, the consideration of the *mutual* interaction between the FM and SC elements may be of crucial importance near the transitions. To capture this, we study the current distributions for different applied fields (Fig. 6) and see that for radius $\rho \lesssim R_f$, there is a variation on the currents due to the FM stray field. The destabilizing field for the skyrmion and 2π states are found to vary slightly, on the order of the stray field generated by the magnetic structure ($\simeq \pm 0.05 M_s$). This effect becomes more relevant as the interaction between elements is more relevant. Thus, it becomes clear that even for cases in which the FM and SC are at a considerable distance (compared to R_f), the effects of the mutual interaction might be critical to correctly characterize the energy landscape and stability of the system under study.

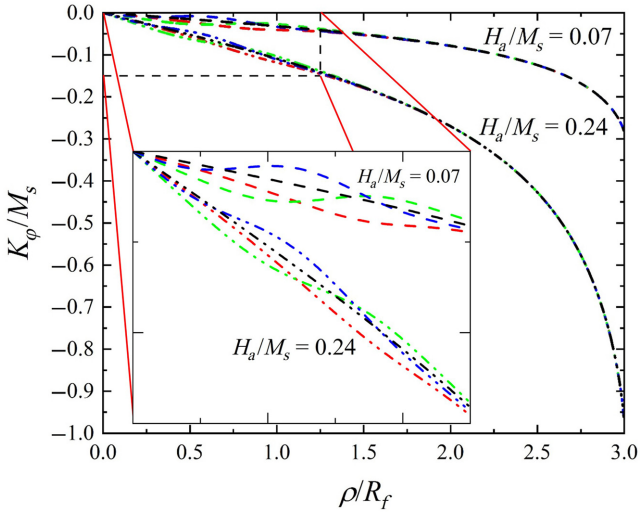

FIG. 6. The current distribution for different applied fields when the superconducting currents are not affected by the FM (black) or are affected by a (quasi)uniform (red), skyrmion (green), or 2π (blue) state. For $\rho \simeq R_f$, the currents vary significantly. The inset shows an enlargement of the marked region of the main plot.

C. Dependence on parameters

It is also important to discuss the relevance of some of the parameters to assess the generality of the presented results.

For a small enough FM radius, there is no space to host the twisting of the magnetization and the skyrmion or 2π distributions are no longer possible. In the opposite limit, for large R_f, 3π or 4π states could also be stabilized [10] (in general, these states would be more difficult to reach and stabilize). When several states are possible inside a FM (as in the example shown), the magnetization distribution of each state is strongly dependent on R_f, shrinking when R_f decreases (until disappearance, if there is no space for that distribution). We calculate the interaction using several values of R_f and find that the general trends described above also hold (when comparison is possible).

In all the presented results, we use $\Lambda = 24$ nm. In the $\Lambda = 0$ limit, the shielding is perfect, the magnetic induction field $\mathbf{B} = 0$ inside the superconductor, and the field lines surround the SC plane. For $\Lambda > 0$, there is a shielding effect, but it is not perfect. Roughly speaking, the larger the Λ, the less excluded the magnetic field is from its interior. If Λ was very large, compared to R_f, the SC would produce no effect.

Regarding the election of parameters for the FM, we recalculate the states using Pt/Co parameters [59], finding similar results (with some variation in the particular values of magnitudes, in particular the ranges of applied fields of stability of the different states).

V. CONCLUSIONS

We study the interaction between a FM and a SC taking into account the mutual stray field produced by the ferromagnetic magnetization distribution and the induced superconducting currents. We solve numerically the equations describing the SC (the London equation, within the London approximation) and the FM (the Brown equation, within the micromagnetic model) simultaneously. The results obtained could be useful from several points of view.

First, the presented model is easily extensible to other systems. For example, the introduction of superconducting vortices is straightforward by including an extra term in the London equation. In addition, the consideration of several layers would be straightforward, through solving all of them simultaneously.

Second, the presence of three (or more) differentiated states of magnetization, stable over a large applied field range and accessible at will, could be used for the design of ternary-logic systems that could allow new computation schemes, as well as increasing the density of stored information, not by increasing the density of dots, but the allowed number of states per dot.

Third, the precise knowledge of the interaction between a FM and a SC is not only interesting from the fundamental point of view but it could serve as starting point in the study of more complex systems made by quasirepetition of FM/SC bilayers. More precisely, repetitions of bilayers varying the distance between the ferromagnetic and superconducting layers or varying the distance between the bilayers could be simulated. In this line, one could envisage "skyrmionic metamaterials," where the effective magnetic properties (i.e., the effective permeability) could be tuned, even in an nonuniform and/or nonisotropic way.

ACKNOWLEDGMENTS

We acknowledge Catalan project 2017-SGR-105 and Spanish project PID2019-104670GB-I00 of the Agencia Estatal de Investigación−Fondo Europeo de Desarrollo Regional (UE) for financial support. J.C.-Q. acknowledges Grant No. FPU17/01970 from the Ministerio de Ciencia, Innovación y Universidades (Spanish Government).

[1] I. F. Lyuksyutov and V. L. Pokrovsky, Ferromagnet-superconductor hybrids, Adv. Phys. **54**, 67 (2005).

[2] A. Palau, S. Valencia, N. Del-Valle, C. Navau, M. Cialone, A. Arora, F. Kronast, D. A. Tennant, X. Obradors, A. Sanchez, and T. Puig, Encoding magnetic states in monopole-like configurations using superconducting dots, Adv. Sci. **3**, 1600207 (2016).

[3] V. K. Vlasko-Vlasov, F. Colauto, A. I. Buzdin, D. Rosenmann, T. Benseman, and W.-K. Kwok, Manipulating Abrikosov vortices with soft magnetic stripes, Phys. Rev. B **95**, 174514 (2017).

[4] A. Stellhorn, A. Sarkar, E. Kentzinger, J. Barthel, A. D. Bernardo, S. Nandi, P. Zakalek, J. Schubert, and T. Brückel, Tailoring superconducting states in superconductor-ferromagnet hybrids, New J. Phys. **22**, 093001 (2020).

[5] V. N. Kushnir, S. L. Prischepa, M. Trezza, C. Cirillo, and C. Attanasio, Superconducting order parameter nucleation and critical currents in the presence of weak stray fields in superconductor/insulator/ferromagnet hybrids, Coatings **11**, 507 (2021).

[6] A. Fert, V. Cros, and J. Sampaio, Skyrmions on the track., Nat. Nanotechnol. **8**, 152 (2013).

[7] X. Ma, G. Yu, X. Li, T. Wang, D. Wu, K. S. Olsson, Z. Chu, K. An, J. Q. Xiao, K. L. Wang, and X. Li, Interfacial control of Dzyaloshinskii-Moriya interaction in heavy metal/ferromagnetic metal thin film heterostructures, Phys. Rev. B **94**, 180408 (2016).

[8] S. Woo, K. Litzius, B. Krüger, M.-Y. Im, L. Caretta, K. Richter, M. Mann, A. Krone, R. M. Reeve, M. Weigand, P. Agrawal, I. Lemesh, M.-A. Mawass, P. Fischer, M. Kläui, and G. S. D. Beach, Observation of room-temperature magnetic skyrmions and their current-driven dynamics in ultrathin metallic ferromagnets, Nat. Mater. **15**, 501 (2016).

[9] C. Moreau-Luchaire, C. Moutafis, N. Reyren, J. Sampaio, C. A. F. Vaz, N. Van Horne, K. Bouzehouane, K. Garcia,

C. Deranlot, P. Warnicke, P. Wohlhüter, J.-M. George, M. Weigand, J. Raabe, V. Cros, and A. Fert, Additive interfacial chiral interaction in multilayers for stabilization of small individual skyrmions at room temperature, Nat. Nanotechnol. **11**, 444 (2016).

[10] S. Rohart and A. Thiaville, Skyrmion confinement in ultrathin film nanostructures in the presence of Dzyaloshinskii-Moriya interaction, Phys. Rev. B **88**, 184422 (2013).

[11] M. A. Castro and S. Allende, Skyrmion core size dependence as a function of the perpendicular anisotropy and radius in magnetic nanodots, J. Magn. Magn. Mater. **417**, 344 (2016).

[12] X. Zhao, C. Jin, C. Wang, H. Du, J. Zang, M. Tian, R. Che, and Y. Zhang, Direct imaging of magnetic field-driven transitions of skyrmion cluster states in FeGe nanodisks, Proc. Natl. Acad. Sci. **113**, 4918 (2016).

[13] J. Mulkers, M. V. Milošević, and B. Van Waeyenberge, Cycloidal versus skyrmionic states in mesoscopic chiral magnets, Phys. Rev. B **93**, 214405 (2016).

[14] R. Juge, S. G. Je, D. de Souza Chaves, S. Pizzini, L. D. Buda-Prejbeanu, L. Aballe, M. Foerster, A. Locatelli, T. O. Menteş, A. Sala, F. Maccherozzi, S. S. Dhesi, S. Auffret, E. Gautier, G. Gaudin, J. Vogel, and O. Boulle, Magnetic skyrmions in confined geometries: Effect of the magnetic field and the disorder, J. Magn. Magn. Mater. **455**, 3 (2018).

[15] D. Cortés-Ortuño, N. Romming, M. Beg, K. Von Bergmann, A. Kubetzka, O. Hovorka, H. Fangohr, and R. Wiesendanger, Nanoscale magnetic skyrmions and target states in confined geometries, Phys. Rev. B **99**, 214408 (2019).

[16] H. Li, C. A. Akosa, P. Yan, Y. Wang, and Z. Cheng, Stabilization of Skyrmions in a Nanodisk without an External Magnetic Field, Phys. Rev. Appl. **13**, 034046 (2020).

[17] M. Tinkham, *Introduction to Superconductivity* (Dover Publications, New York, 2004), 2nd ed.

[18] P. G. De Gennes, *Superconductivity of Metals and Alloys* (CRC Press, Boca Raton, 1999), 1st ed.

[19] Z. Yang, M. Lange, A. Volodin, R. Szymczak, and V. V. Moshchalkov, Domain-wall superconductivity in superconductor-ferromagnet hybrids, Nat. Mater. **3**, 793 (2004).

[20] C. Jooss, J. Albrecht, H. Kuhn, S. Leonhardt, and H. Kronmüller, Magneto-optical studies of current distributions in high-T_c superconductors, Rep. Prog. Phys. **65**, 651 (2002).

[21] J. E. Villegas, S. Savel'ev, F. Nori, E. M. Gonzalez, J. V. Anguita, R. García, and J. L. Vicent, A superconducting reversible rectifier that controls the motion of magnetic flux quanta, Science **302**, 1188 (2003).

[22] N. Del-Valle, S. Agramunt-Puig, A. Sanchez, and C. Navau, Imprinting skyrmions in thin films by ferromagnetic and superconducting templates, Appl. Phys. Lett. **107**, 133103 (2015).

[23] M. Garnier, A. Mesaros, and P. Simon, Topological superconductivity with deformable magnetic skyrmions, Commun. Phys. **2**, 126 (2019).

[24] E. Mascot, J. Bedow, M. Graham, S. Rachel, and D. K. Morr, Topological superconductivity in skyrmion lattices, Npj Quantum Mater. **6**, 6 (2021).

[25] S. Rex, I. V. Gornyi, and A. D. Mirlin, Majorana bound states in magnetic skyrmions imposed onto a superconductor, Phys. Rev. B **100**, 064504 (2019).

[26] I. F. Lyuksyutov and V. Pokrovsky, Magnetization Controlled Superconductivity in a Film with Magnetic Dots, Phys. Rev. Lett. **81**, 2344 (1998).

[27] J. Baumard, J. Cayssol, F. S. Bergeret, and A. Buzdin, Generation of a superconducting vortex via Néel skyrmions, Phys. Rev. B **99**, 014511 (2019).

[28] M. V. Milošević and F. M. Peeters, Interaction between a superconducting vortex and an out-of-plane magnetized ferromagnetic disk: Influence of the magnet geometry, Phys. Rev. B **68**, 094510 (2003).

[29] S. Erdin, I. F. Lyuksyutov, V. L. Pokrovsky, and V. M. Vinokur, Topological Textures in a Ferromagnet-Superconductor Bilayer, Phys. Rev. Lett. **88**, 017001 (2001).

[30] R. Laiho, E. Lähderanta, E. B. Sonin, and K. B. Traito, Penetration of vortices into the ferromagnet/type-II superconductor bilayer, Phys. Rev. B **67**, 144522 (2003).

[31] K. M. Hals, M. Schecter, and M. S. Rudner, Composite Topological Excitations in Ferromagnet-Superconductor Heterostructures, Phys. Rev. Lett. **117**, 017001 (2016).

[32] S. M. Dahir, A. F. Volkov, and I. M. Eremin, Interaction of Skyrmions and Pearl Vortices in Superconductor-Chiral Ferromagnet Heterostructures, Phys. Rev. Lett. **122**, 097001 (2019).

[33] R. M. Menezes, J. F. Neto, C. C. S. Silva, and M. V. Milošević, Manipulation of magnetic skyrmions by superconducting vortices in ferromagnet-superconductor heterostructures, Phys. Rev. B **100**, 014431 (2019).

[34] X. Palermo, N. Reyren, S. Mesoraca, A. V. Samokhvalov, S. Collin, F. Godel, A. Sander, K. Bouzehouane, J. Santamaria, V. Cros, A. I. Buzdin, and J. E. Villegas, Tailored Flux Pinning in Superconductor-Ferromagnet Multilayers with Engineered Magnetic Domain Morphology from Stripes to Skyrmions, Phys. Rev. Appl. **13**, 014043 (2020).

[35] A. I. Buzdin, Proximity effects in superconductor-ferromagnet heterostructures, Rev. Mod. Phys. **77**, 935 (2005).

[36] S. M. Dahir, A. F. Volkov, and I. M. Eremin, Meissner currents induced by topological magnetic textures in hybrid superconductor/ferromagnet structures, Phys. Rev. B **102**, 014503 (2020).

[37] V. L. Vadimov, M. V. Sapozhnikov, and A. S. Mel'nikov, Magnetic skyrmions in ferromagnet-superconductor (F/S) heterostructures, Appl. Phys. Lett. **113**, 032402 (2018).

[38] E. S. Andriyakhina and I. S. Burmistrov, Interaction of a Néel-type skyrmion with a superconducting vortex, Phys. Rev. B **103**, 174519 (2021).

[39] A. P. Petrović, M. Raju, X. Y. Tee, A. Louat, I. Maggio-Aprile, R. M. Menezes, M. J. Wyszyński, N. K. Duong, M. Reznikov, C. Renner, M. V. Milošević, and C. Panagopoulos, Skyrmion-(Anti)vortex Coupling in a Chiral Magnet-Superconductor Heterostructure, Phys. Rev. Lett. **126**, 117205 (2021).

[40] Y. Liu and X. Zhang, Metamaterials: A new frontier of science and technology, Chem. Soc. Rev. **40**, 2494 (2011).

[41] A. Sanchez, C. Navau, J. Prat-Camps, and D.-X. Chen, Antimagnets: Controlling magnetic fields with

superconductor-metamaterial hybrids, New J. Phys. **13**, 093034 (2011).

[42] J. Pearl, Structure of superconductive vortices near a metal-air interface, J. Appl. Phys. **37**, 4139 (1966).

[43] J. R. Kirtley, C. C. Tsuei, V. G. Kogan, J. R. Clem, H. Raffy, and Z. Z. Li, Fluxoid dynamics in superconducting thin film rings, Phys. Rev. B **68**, 214505 (2003).

[44] J. Mulkers, B. Van Waeyenberge, and M. V. Milošević, Effects of spatially engineered Dzyaloshinskii-Moriya interaction in ferromagnetic films, Phys. Rev. B **95**, 144401 (2017).

[45] J. Castell-Queralt, L. González-Gómez, N. Del-Valle, A. Sanchez, and C. Navau, Accelerating, guiding, and compressing skyrmions by defect rails, Nanoscale **11**, 12589 (2019).

[46] J. M. D. Coey, *Magnetism and Magnetic Materials* (Cambridge University Press, New York, 2010).

[47] H. Kronmuller and M. Fahnle, *Micromagnetism and the Microstructure of Ferromagnetic Solids* (Cambridge University Press, New York, 2003), p. 432.

[48] E. H. Brandt and J. R. Clem, Superconducting thin rings with finite penetration depth, Phys. Rev. B—Condens. Matter Mater. Phys. **69**, 184509 (2004).

[49] J. Castell-Queralt, L. González-Gómez, N. Del-Valle, and C. Navau, Exploiting symmetries in skyrmionic micromagnetic simulations: Cylindrical and radial meshes, J. Magn. Magn. Mater. **549**, 168972 (2022).

[50] A. Cao, R. Chen, X. Wang, X. Zhang, S. Lu, S. Yan, B. Koopmans, and W. Zhao, Enhanced interfacial Dzyaloshinskii-Moriya interactions in annealed Pt/Co/MgO structures, Nanotechnology **31**, 155705 (2020).

[51] C. Kittel, *Introduction to Solid State Physics* (John Wiley & Sons, 1996) Chap. 12, p. 352.

[52] H.-B. Braun, Topological effects in nanomagnetism: From superparamagnetism to chiral quantum solitons, Adv. Phys. **61**, 1 (2012).

[53] W. Jiang, G. Chen, K. Liu, J. Zang, S. G. te Velthuis, and A. Hoffmann, Skyrmions in magnetic multilayers, Phys. Rep. **704**, 1 (2017), skyrmions in Magnetic Multilayers.

[54] P. F. Bessarab, V. M. Uzdin, and H. Jónsson, Method for finding mechanism and activation energy of magnetic transitions, applied to skyrmion and antivortex annihilation, Comput. Phys. Commun. **196**, 335 (2015).

[55] F. Muckel, S. von Malottki, C. Holl, B. Pestka, M. Pratzer, P. F. Bessarab, S. Heinze, and M. Morgenstern, Experimental identification of two distinct skyrmion collapse mechanisms, Nat. Phys. **17**, 395 (2021).

[56] P. F. Bessarab, G. P. Müller, I. S. Lobanov, F. N. Rybakov, H. Kiselev, N. S. Jónsson, V. M. Uzdin, S. Blügel, L. Bergqvist, and A. Delin, Lifetime of racetrack skyrmions, Sci. Rep. **8**, 3433 (2018).

[57] D. Cortés-Ortuño, W. Wang, M. Beg, R. A. Pepper, M.-A. Bisotti, R. Carey, M. Vousden, T. Kluyver, O. Hovorka, and H. Fangohr, Thermal stability and topological protection of skyrmions in nanotracks, Sci. Rep. **7**, 4060 (2017).

[58] See the Supplemental Material at http://link.aps.org/supplemental/10.1103/PhysRevApplied.17.034069 for videos with the magnetization distributions along the magnetization loop.

[59] C. Song, C. Jin, J. Wang, H. Xia, J. Wang, and Q. Liu, Appl. Phys. Lett. **111**, 19213 (2017).